ISSN 1063-7729, Astronomy Reports, 2021, Vol. 65, No. 12, pp. 1233–1245. © Pleiades Publishing, Ltd., 2021.
Russian Text © The Author(s), 2021, published in Astronomicheskii Zhurnal, 2021, Vol. 98, No. 12, pp. 997–1009.

Variability of the Blazar 1156+295 in 2005–2020

V. A. Hagen-Thorn[a, *], D. A. Morozova[b], S. S. Savchenko[a], E. I. Hagen-Thorn[c], Yu. V. Milanova[a], L. V. Shalyapina[a], and A. A. Vasil'ev[b]

[a] *Astrophysics Chair, Saint Petersburg State University, Saint Petersburg, Russia*
[b] *Laboratory of Observational Astrophysics, Saint Petersburg State University, Saint Petersburg, Russia*
[c] *Main (Pulkovo) Astronomical Observatory, RAS, Saint Petersburg, Russia*
**e-mail: hth-home@yandex.ru*

Received May 4, 2021; revised July 15, 2021; accepted July 27, 2021

Abstract—We present and analyze the monitoring results of the blazar 1156+295 in radio, optical, and gamma ranges in 2005–2020. After a long period of relative quietness at the end of 2017, a sharp increase in activity occurred in all spectral ranges, from radio to gamma. The connection between events that took place in different ranges has been studied. Photometric variability in the optical-infrared region is explained by the presence of a variable component with a constant on average power-law relative energy distribution in the spectrum ($F_\nu \sim \nu^{-1.4}$). Separate sources of polarized radiation with a relatively high degree of polarization are identified. The synchrotron nature of the components responsible for the activity is beyond doubt. During VLBI observations, four components moving at superluminal speeds were found; a connection has been established between the instants of their appearance and events in all spectral ranges. It is noted that the difference in the values of the spectral indices for different time intervals does not allow to explain the variability of the flux by geometric factors only (by the change in the Doppler factor due to the change in the angle between the line of sight and the subluminal motion direction of the emitting ensemble of electrons). For different time intervals, the energy distributions of electrons in ensembles should be different.

Keywords: blazars, variability, photometry, polarimetry, radio-structure

DOI: 10.1134/S1063772921120039

1. INTRODUCTION

The blazar 1156+295 ($z = 0.729$ [1]), which shows flux variability in all ranges of the electromagnetic spectrum from radio to gamma, has been studied already for several decades. In the optical range of the spectrum, the first results of its five-color observations [2, 3] showed the variability of the flux between January 8, 1983 and June 14, 1984 and a high degree of polarization. An analysis of these photometric data was carried out in [4], where the power-law character of the spectrum of the source responsible for the variability was found. A high degree of radiation polarization made it possible to draw a conclusion about its synchrotron nature.

There are many papers reporting study results of the object in the radio range; among them are both monitoring[1] and VLBI observations [5]. The radiation of the object in the gamma range was recorded by the Fermi space observatory [6].

In this paper, we present the results of optical and IR monitoring observations of the blazar 1156+295 conducted at St. Petersburg (StPSU) and Boston Universities and their analysis, the results of VLBI observations obtained by the Boston University group and their analysis (a continuation of the studies published in [5]), as well as the comparison of the features of variability in different spectral ranges.

2. OBSERVATIONAL DATA

In St. Petersburg State University, photometric observations in the *B, V, R, I* bands were carried out at the 70-cm telescope of the Crimean Astrophysical Observatory and at the 40-cm telescope of the Astronomical Institute of St. Petersburg University, equipped by identical CCD photometers-polarimeters. Observations and processing technique are described in [7]. The Boston University team carried out observations in the same spectral bands at the 1.8-m Perkins telescope of Lowell Observatory (Flagstaff, Arizona) with a PRISM photometer-polarimeter [8]. Also, publicly available data obtained at Steward Observatories (http://james.as.arizona.edu/psmith/Fermi/) were used. There are no systematic differences between the observation series. The errors of photometric estimates do not exceed 0.03^m.

[1] http://www.astro.lsa.umich.edu/obs/radiotel/umrao.php

Observations in the IR range (bands *J, H, K*) were made at the Campo-Imperatore observatory using the 1.2-m telescope with a SWIRCAM camera. The method of observations and processing techniques are described in [7].

To change from the stellar magnitudes to the flux densities used in further analysis, we used the calibration from [9] (hereinafter, for brevity, instead of "flux density," we will use "flux"). Flux values averaged over JD are shown in Fig. 1. In the panel most filled by observations in the *R* band, it can be seen that the flux at the maximum is almost 50 times higher than the minimum values. It can be seen that the nature of the flow change was different in 2006–2016 and 2017–2019. During the first time span, the minimum flux was maintained, interrupted by individual flashes of moderate intensity; in the second time span, the object demonstrates violent activity.

Polarization measurements were carried out either in the *R* band (at 70-cm and 1.8-m telescopes) or in a wide band with an effective wavelength close to the wavelength for the *R* band (at a 40-cm telescope). The technique of polarization observations and processing is described in [7, 8]. For most of the observations, errors of the degree and direction of polarization do not exceed 2% and several degrees, respectively. Results of polarization observations are shown in Fig. 2 in the first two panels (in the third, for convenience of comparison, the light curve in the *R*-band is shown). It is seen that the degree of polarization varies within wide limits, reaching a maximum of 43%; among the directions of polarization, all possible values are found and no clear predominant direction is observed.

For the analysis in the gamma-range, we used the data obtained by the Fermi space observatory in the range of 0.1–200 GeV. The processing was performed using standard software [10]. The results obtained using adaptive binning are shown in the lower panel of Fig. 3 (together with the light curve in the *R*-band, for the ease of comparison).

The object 1156 + 295 is included into the sample of gamma-bright blazars, for which the group from Boston University is conducting monitoring observations by the VLBA network at 43 GHz (data for all epochs are available at http://www.bu.edu/blazars/VLBAproject.html). The used VLBA data were calibrated and processed by the method described in [11]. We used the observation results in the full stream for 66 epochs between February 26, 2013 and January 1, 2020. Each image was simulated by a set of components with a circular Gaussian distribution of brightness in the Difmap software package. These results were further used to study the jet kinematics.

3. THE ANALYSIS OF PHOTOMETRIC DATA

Since the light curve of 1156+295 shows a change of the nature of variability close to JD 2457650, we first performed a periodicity analysis for the series limited by this date. We used data for the *R*-band, in which the most numerous observations appeared. The Lomb-Scargle periodogram, which is widely used for the search of periodicity in uneven time series was constructed. The calculation result of the periodogram is shown in Fig. 4 (bottom panel). Since the observed periodogram is a convolution of the true periodogram and the tapering function, Fig. 4 also contains the periodogram of the latter (top panel). The periodogram of the tapering function has a peak at the frequency 0.00274 day^{-1} (period 364.96 day, the annual observations duty cycle). The periodogram of the light curve has two peaks: the highest at the frequency of 0.00132 day^{-1} (period 757.6 day) and the second highest at the frequency of 0.00400 day^{-1} (period 250.0 day). Thus, the frequency of the second peak with good accuracy coincides with the sum of the frequencies of the first peak and the peak in the periodogram of the tapering function (0.00132+0.00274 = 0.00406); this indicates that the second peak is false. Note that the period close to the one derived by us was found from the results of radio observations in [12]. After JD 2457650, this periodicity is violated.

Observed changes in the brightness of blazars, as a rule, are accompanied by the changes of the color indices, which are often associated with the color variability of the source responsible for the activity. However, it easy to understand that, in the case of difference in the energy distribution in the spectra of continuous and variable components, observed variability of colors may be explained by the contribution variability of variable components in the total observed radiation. Incorrect account of the contribution of the *unobservable directly* constant component leads to an erroneous determination of the variable component contribution. This leads to the incorrect determination of the properties of the source responsible for activity.

In this regard, it is important to obtain information on the color characteristics of the source responsible for the activity *directly* from the photometric data obtained during observations. Sometimes this is possible. Corresponding data analysis technique is described in detail in [13], and the results of its successful application to the study of blazars have been published in a number of papers (for example, [14, 15]).

The essence of the method is construction of "flux–flux" diagrams for a pair of strips, in which the points representing simultaneous observations in the case of *permanence of the color characteristics* of the variable component over given time interval lie on the straight lines. The converse is also true. Location of the points on the straight lines indicates the perma-

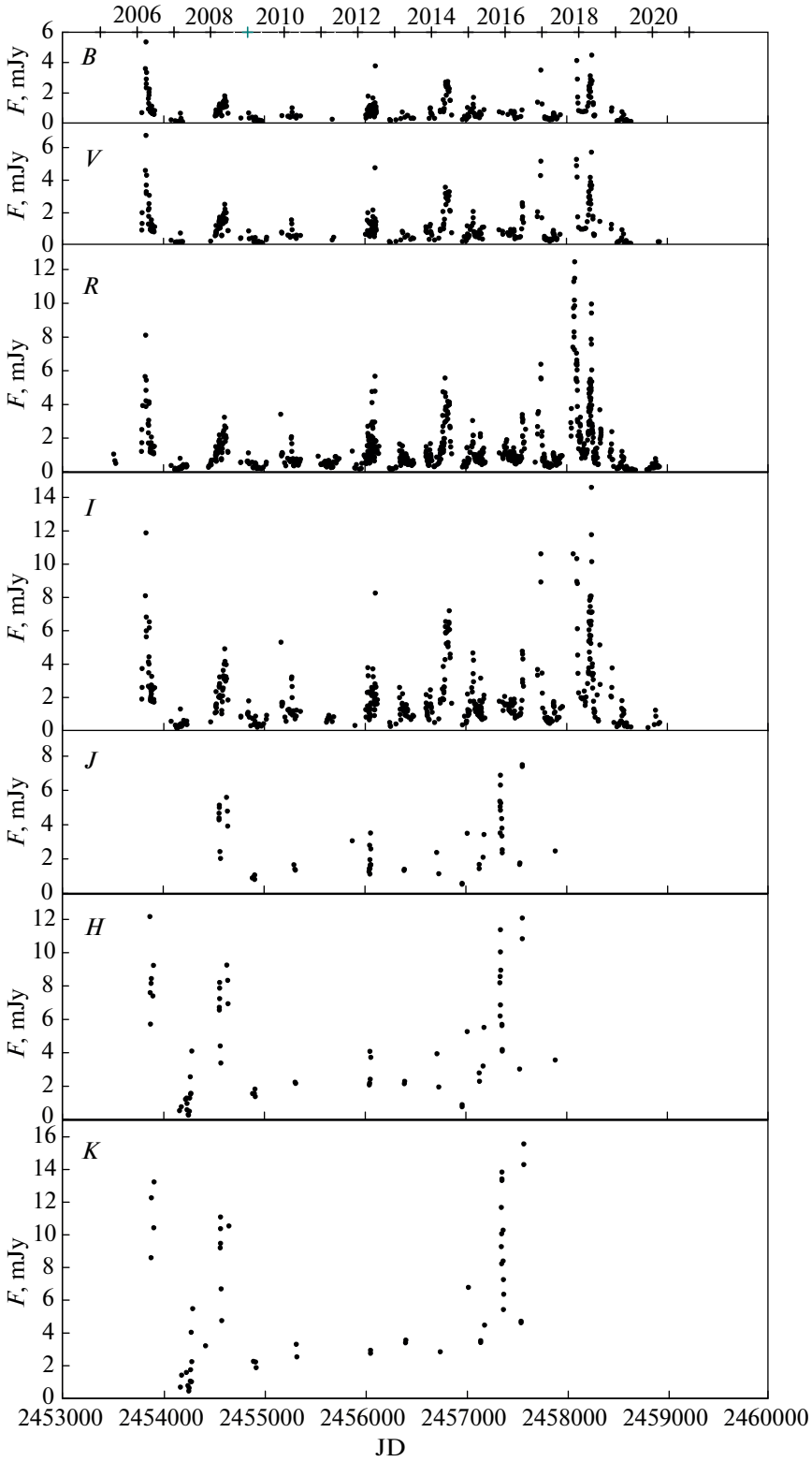

Fig. 1. Variability of 1156+295 in the visual-infrared range of spectrum.

nence of the color characteristics of the variable component, and the slopes of the straight lines give the ratio of the *variable component* fluxes in the bands under consideration. Multicolor observations of variability thus give a relative energy distribution in the spectrum of the *variable* component. Deviation of the

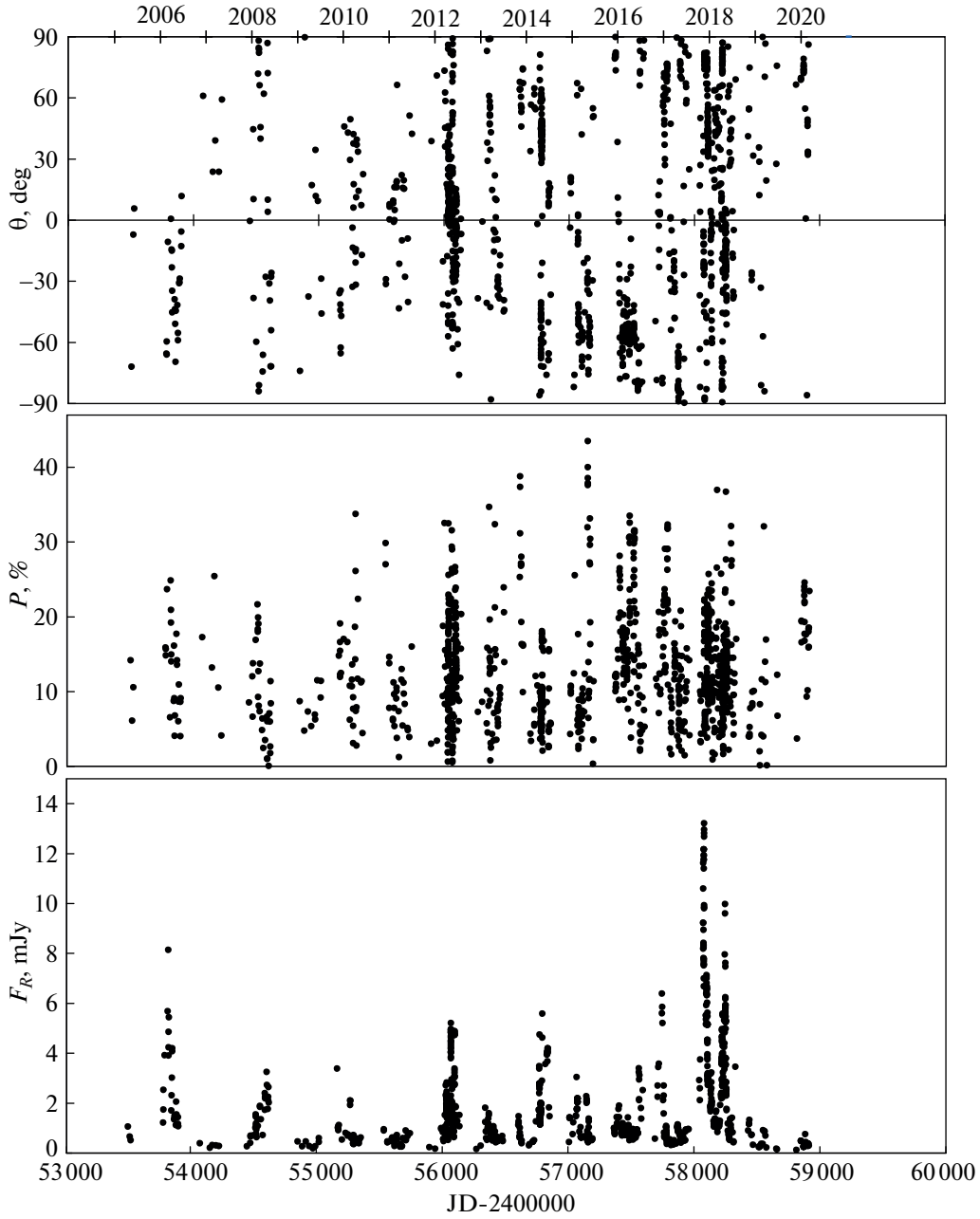

Fig. 2. Results of polarization measurements in *R*-band.

points from the straight lines indicates a change of the color characteristics of the variable component at the given time interval; in this case, the method is not applicable.

The "flux–flux" diagrams for the entire set of observational data are shown in Fig. 5. The bands *R* (in the visual region of the spectrum) and *K* (in the infrared one) were selected as the base bands. It can be seen that the relationship between the fluxes is linear, that is, the variable component, *on average*, does not change its energy distribution in the spectrum. The following equations of straight lines were obtained by the method of orthogonal regression (the errors of the coefficients at the 1σ level are indicated in parentheses. After each of the equations, the number of points used to determine the coefficients of the equation *n* and the correlation coefficients *r* are indicated):

$$F_B = 0.596(\pm 0.005)F_R + 0.028(\pm 0.010),$$
$$n = 285, \quad r = 0.988;$$

$$F_V = 0.787(\pm 0.003)F_R + 0.021(\pm 0.007),$$
$$n = 329, \quad r = 0.995;$$

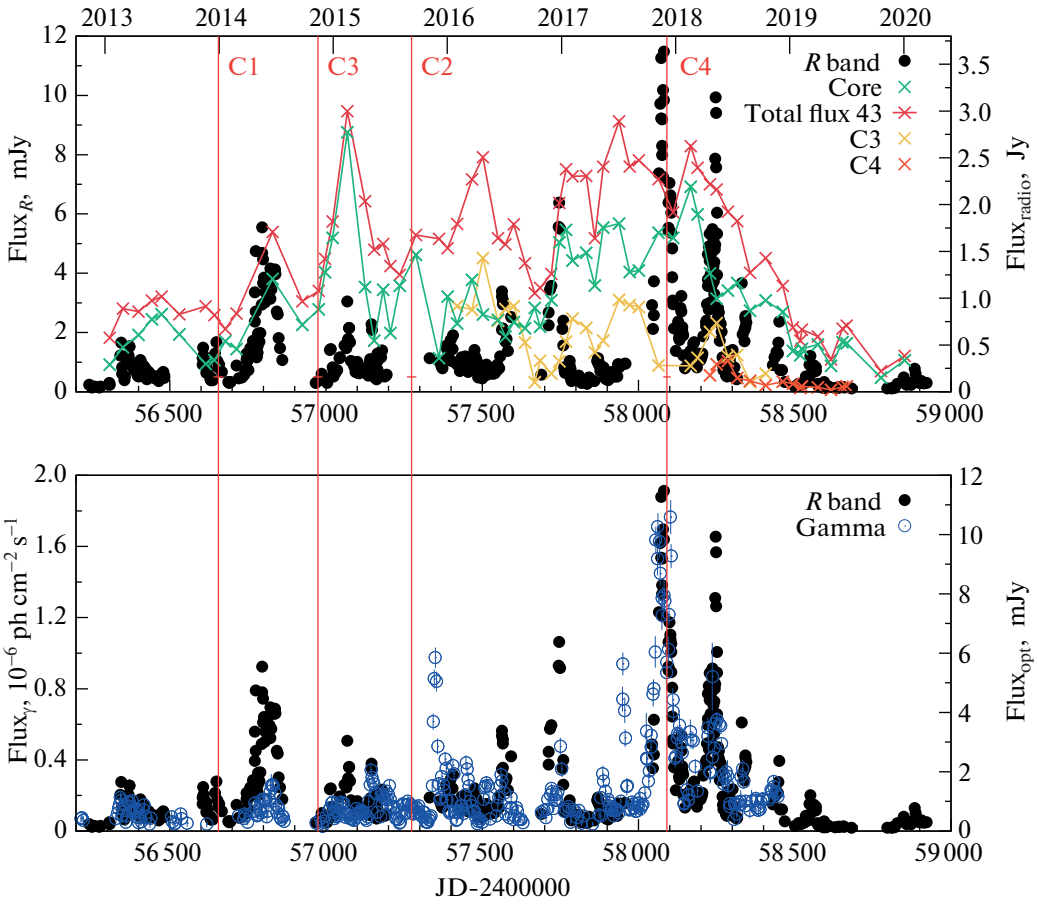

Fig. 3. Comparison of variability of 1156+295 in different ranges.

$$\begin{gathered} F_I = 1.511(\pm0.004)F_R + 0.001(\pm0.008), \\ n = 480, \quad r = 0.995; \\ F_K = 5.786(\pm0142)F_R - 0.158(\pm0.224), \\ n = 12, \quad r = 0.890; \\ F_J = 0.484(\pm0.015)F_K - 0.219(\pm0.124), \\ n = 37, \quad r = 0.979; \\ F_H = 0.702(\pm0.019)F_K + 0.090(\pm0.154), \\ n = 51, \quad r = 0.974. \end{gathered} \tag{1}$$

The fourth equation of the system connects optical and infrared data by substituting it into the fifth and sixth equations.

The slopes of the straight lines provide the ratio of the fluxes of the variable component, that is, the *average observed* relative energy distribution in its spectrum for the considered time interval. It is presented in the third column of Table 1. The resulting distribution should be corrected for the interstellar extinction in the Galaxy. Thus, the values from the third column of the Table 1 were multiplied by the coefficients C_{iR}, where $\log_{10}C_{iR} = 0.4\ (Ai - A_R)$. Absorption values A_i were taken from the NED database (https://ned.ipac.caltech.edu/). Since interstellar absorption is small, the corrected energy distribution differs little from the observed one; the former is presented in the fifth column of Table 1. In the logarithmic scale, both distributions are presented in the sixth and seventh columns of the table. Figure 6 (dots, right ordinate scale) shows the distribution corrected for absorption. It is seen that the energy distribution in the spectrum of the variable component is a power law $F_\nu \sim \nu^\alpha$. The line obtained by the least squares method gives the spectral index $\alpha = -1.42 \pm 0.03$.

Let us see how the change in the variable component contribution affects the *observed* energy distribution in the spectrum. For this, using Eqs. (1), we construct the observed energy distribution for the regions close to the minimum ($F_R = 0.5$ mJy) and maximum ($F_R = 10$ mJy) brightness (Fig. 6, left ordinate scale). Spectral indices turn out to be equal to $\alpha = -1.36 \pm 0.06$ and $\alpha = -1.45 \pm 0.03$ for the minimum and maximum, respectively. It can be seen that there is a slight difference in the slopes of the spectrum at minimum (squares) and maximum (triangles) brightness, which means that the object turns slightly more red with increasing brightness, although the variable component, as we found out earlier, does not change color.

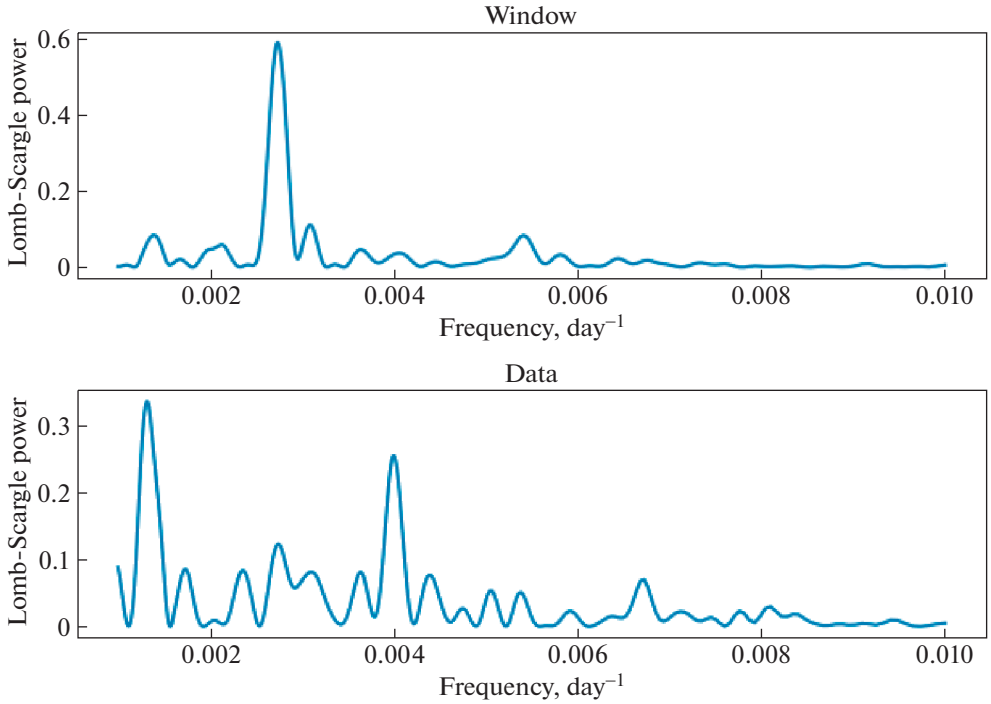

Fig. 4. To the search of periodicity in the brightness variations of 1156+295 in the visual range.

Small color change is due to the proximity of the energy distributions of the constant and variable components. The spectral index at the maximum, as expected, turns out to be close to the spectral index of the variable component, which provides the main contribution to the observed radiation. This proximity is clearly visible in Fig. 6, in which the observed distribution for the variable component (the seventh column of Table 1) is not plotted, since it practically coincides with the one corrected for interstellar absorption.

Earlier studies carried out at St. Petersburg State University have shown that the SED of the variable component in different events can be both different and the same. In this regard, we have determined the spectral indices of the variable component at different observation periods. We used only optical data due to the insufficient number of IR observations. The results are collected in Table 2.

4. THE ANALYSIS OF POLARIZATION DATA

Dependence of the degree of polarization on the brightness is shown in Fig. 7. Noteworthy is the absence of an increase in the degree of polarization with increasing brightness on a global scale, which is often observed in blazars. In the brightest flare, the degree of polarization is only (5–7)%. The behavior of the relative Stokes parameters $\{p_x, p_y\}$ in the diagram confirms the absence of the preferred direction of

Table 1. Determination results of the average relative spectral energy distribution (SED) of the variable component

Band	$\log_{10}\nu$	$(F_i/F_R)^{obs}$	C_{iR}	$(F_i/F_R)^{corr}$	$\log_{10}(F_i/F_R)^{corr}$	$\log_{10}(F_i/F_R)^{obs}$
(1)	(2)	(3)	(4)	(5)	(6)	(7)
B	14.833	0.596 ± 0.005	1.03	0.614 ± 0.005	−0.212 ± 0.004	−0.224 ± 0.004
V	14.736	0.787 ± 0.003	1.01	0.795 ± 0.003	−0.100 ± 0.002	−0.104 ± 0.002
R	14.670	1.0	1.0	1.0	0.0	0.0
I	14.574	1.511 ± 0.004	0.99	1.500 ± 0.004	0.175 ± 0.002	0.179 ± 0.002
J	14.387	2.800 ± 0.143	0.98	2.744 ± 0.140	0.438 ± 0.011	0.447 ± 0.011
H	14.262	4.061 ± 0.144	0.97	3.939 ± 0.141	0.595 ± 0.012	0.609 ± 0.012
K	14.140	5.786 ± 0.142	0.97	5.612 ± 0.138	0.749 ± 0.010	0.762 ± 0.010

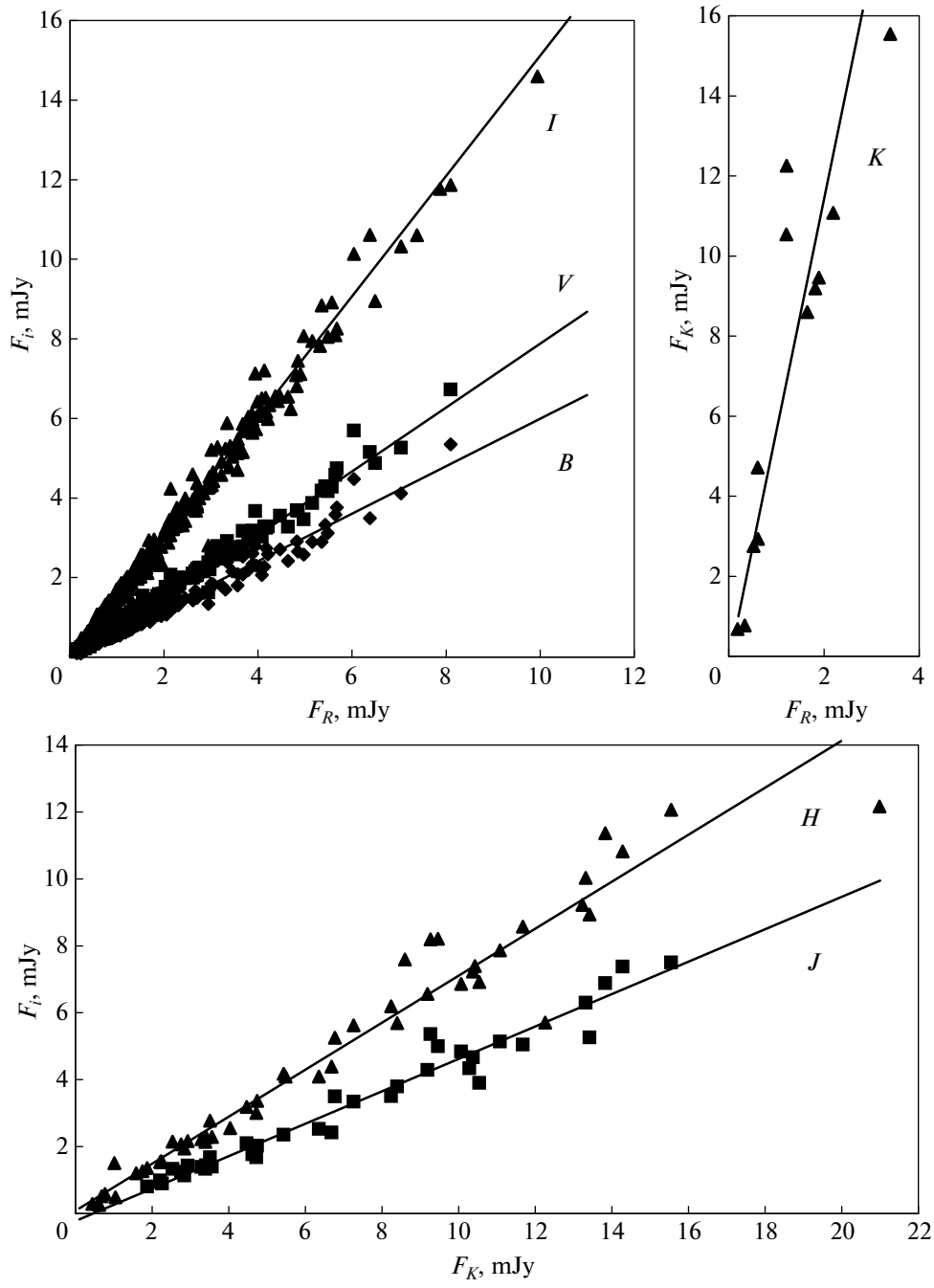

Fig. 5. "Flux–flux" diagrams for entire set of observational data.

polarization of the blazar over entire studied time interval. At the same time, there are distinct structures indicating different polarization behavior of the object at different time intervals.

In the analysis, we used the technique described in [13], where it was shown that there is a fundamental possibility of determination of the polarization parameters of the variable component within the framework of the "constant + variable source" model, if the relative Stokes parameters of the variable component do not change over the considered time interval, and the observed variability of polarization is associated with the change of its contribution to the total radiation only. In this case, in the space of the observed absolute Stokes parameters {*I, Q, U*}, the points representing observations lie on a straight line, the direction tangents of which are the relative Stokes parameters of the variable component. The opposite is also true: location of the points of the straight lines indicates the invariability of the polarization parame-

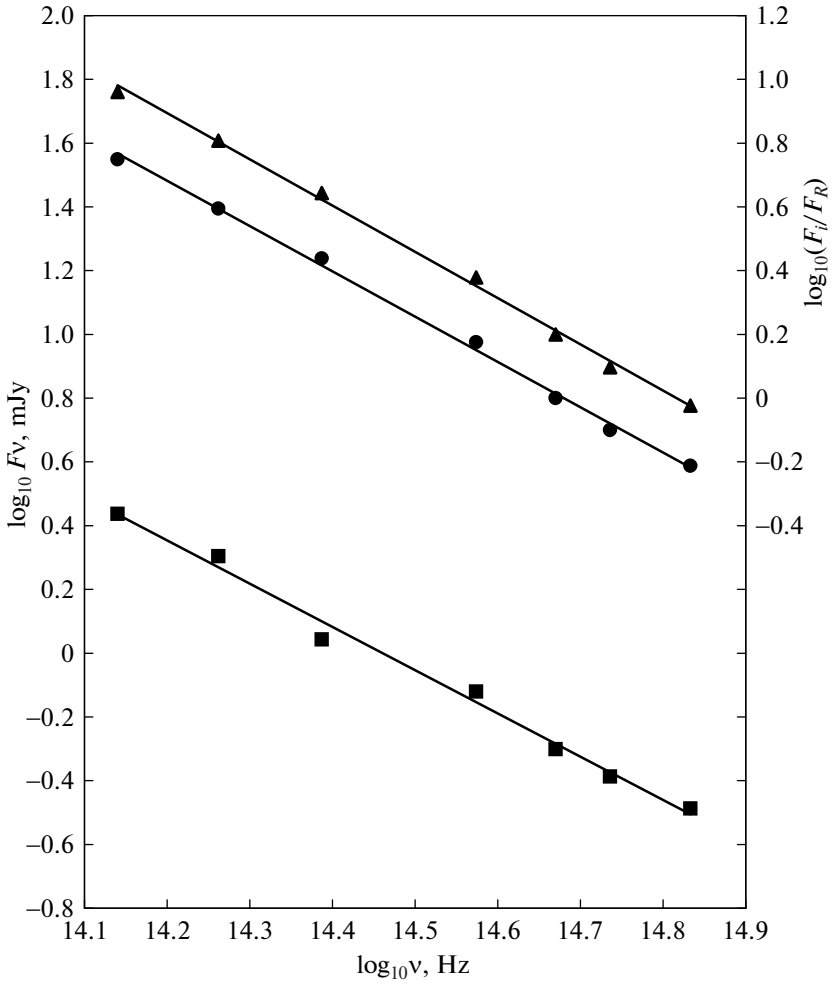

Fig. 6. The spectrum of the variable component and its comparison to the observed spectra.

ters of the variable component and allows them to be determined. In reality, the planes {*I, Q*} and {*I, U*} are considered, in which the points should be located on the straight lines, the slopes of which give the relative Stokes parameters for the variable component $p\nu_x$ and $p\nu_y$, which are then used to find the degree of polarization P_ν and the direction $\theta_{0,\nu}$ of polarization of the variable component.

Since the polarization was measured by us in the *R*-band, the flux in the *I*-band was considered the same. Aside from the rapid changes, we compared the values of F_R, *Q,* and *U* averaged over Julian date. The experience shows that even in the case of short time intervals, the points representing observations rarely appear on the straight lines due to the rapid changes of the polarization parameters of the variable component. In our case, we managed to find several time

Table 2. Spectral indices of relative SED of variable component in the visual range for different time intervals

Interval JD 2450000+	Spectral index	Interval JD 2450000+	Spectral index
3500–4100	-1.25 ± 0.12	6900–7300	-1.50 ± 0.23
4100–4900	-1.63 ± 0.08	7300–7600	-1.08 ± 0.24
4900–5600	-1.69 ± 0.10	7600–8000	-1.75 ± 0.11
5600–6200	-1.27 ± 0.11	8000–8150	-1.52 ± 0.10
6200–6500	-1.45 ± 0.12	8150–8600	-1.52 ± 0.11
6500–6900	-1.51 ± 0.16	Total interval	-1.42 ± 0.03

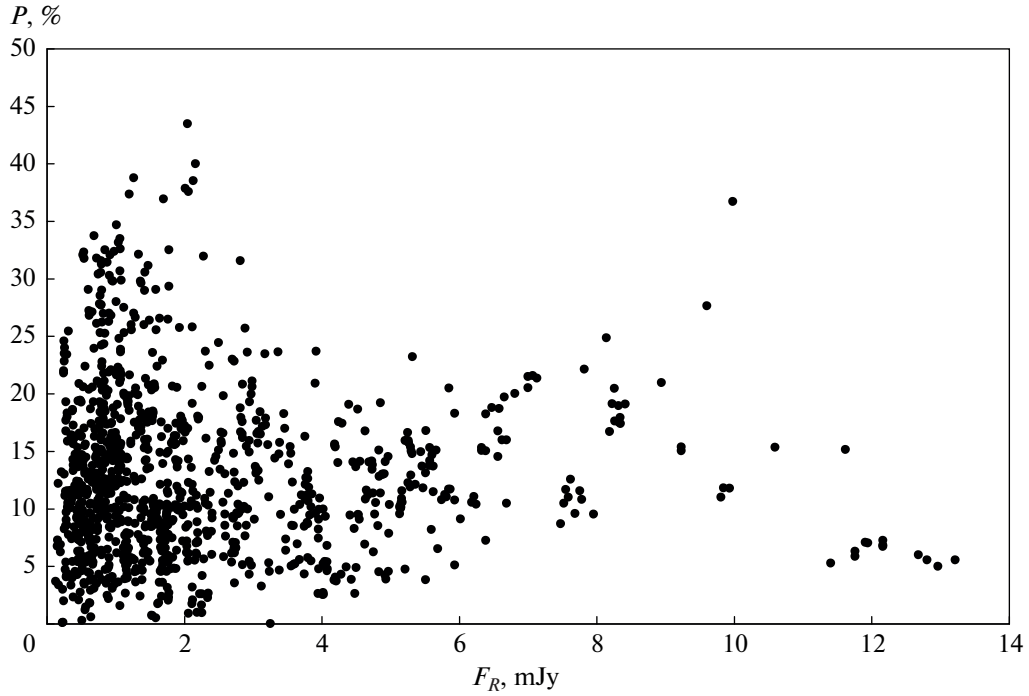

Fig. 7. Dependence of degree of polarization on the observed flux.

intervals for which the points satisfactorily fit the straight lines, although with a large scatter (the examples are shown in Fig. 8). The results are collected in Table 3. The relative Stokes parameters of the variable component found by us, naturally, are related to the *R*-band.

As for the rapid changes (during a night), they are present, but are not large, and the achieved accuracy of polarization observations is not sufficient for a detailed study. However, for a couple of nights, within the framework of the two-component model, it was possible to determine the polarization parameters of the source responsible for the fast variability: 29%, 2° in the range JD2456099 + (0.68–0.79) and 28%, 11° in the range JD2456777 + (0.65–0.87).

5. KINEMATICS AND JET STRUCTURE ACCORDING TO THE VLBI OBSERVATIONS DATA

Consideration of the entire set of images makes it possible to single out individual moving components. In their identification, flux density, positional angle relative to the radio nucleus at 43 GHz, and the distance from it in successive images were considered. In 2013–2020, four moving components (C1, C2, C3, C4) were identified. They appeared between the end of 2013 and the first half of 2018. The motion of the components is illustrated in Fig. 9. The travel times of the components through the radio nucleus at 43 GHz, T_0, found by the linear extrapolation, are shown in Table 4 and are plotted in Fig. 3 by vertical straight lines. In

Table 3. Average values of the polarization parameters of variable component at different time intervals

Interval JD 2450000+	The number of points	$p_{x,v} \pm 1\sigma$	$p_{y,v} \pm 1\sigma$	p_v, %	θ_{0v}, deg
3500–4100	27	0.151 ± 0.031	−0.106 ± 0.017	18.4	−17
4900–5600	37	0.059 ± 0.015	−0.137 ± 0.021	14.9	−33
7064–7103	10	0.150 ± 0.051	−0.079 ± 0.028	17.0	−14
8073–8082	10	−0.410 ± 0.018	0.263 ± 0.072	48.7	74
8095–8111	15	−0.271 ± 0.061	−0.025 ± 0.052	27.2	93
8150–8600	95	0.179 ± 0.018	−0.091 ± 0012	20.1	−14
8239–8259	20	0.296 ± 0.045	−0.055 ± 0.024	30.1	−05

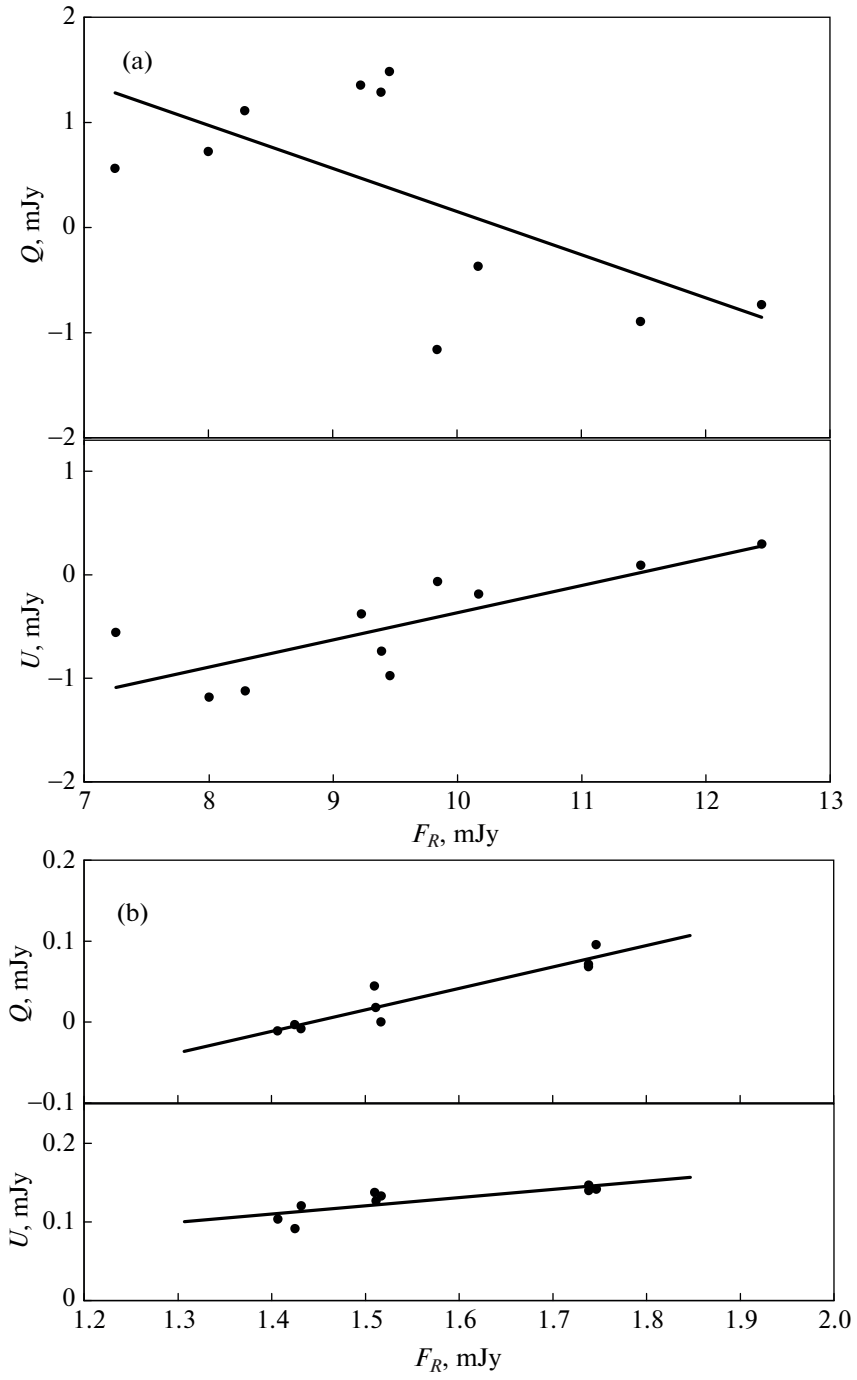

Fig. 8. To the determination of the parameters of polarization of variable components in different events ((a) JD 2458073–8082 and (b) JD 2456777.65–6777.87).

the same table, we present apparent velocities of the components β_{app}, which range from ~*3c* to *13c* (cosmological parameters $H_0 = 70$ km s^{-1} Mpc^{-1}, $\Omega_m = 0.3$, $\Omega_\Lambda = 0.7$ were used), as well as the average fluxes of the components $\langle F \rangle$ and their positional angles $\langle \theta \rangle$ relative to the radio nucleus. The top panel in Fig. 3 (right scale, lines) shows the changes of the fluxes of the entire source, radio nucleus, and components C3 and C4.

6. DISCUSSION OF RESULTS AND CONCLUSIONS

The rise of all four components was accompanied by an increase in the flux density in the radio nucleus,

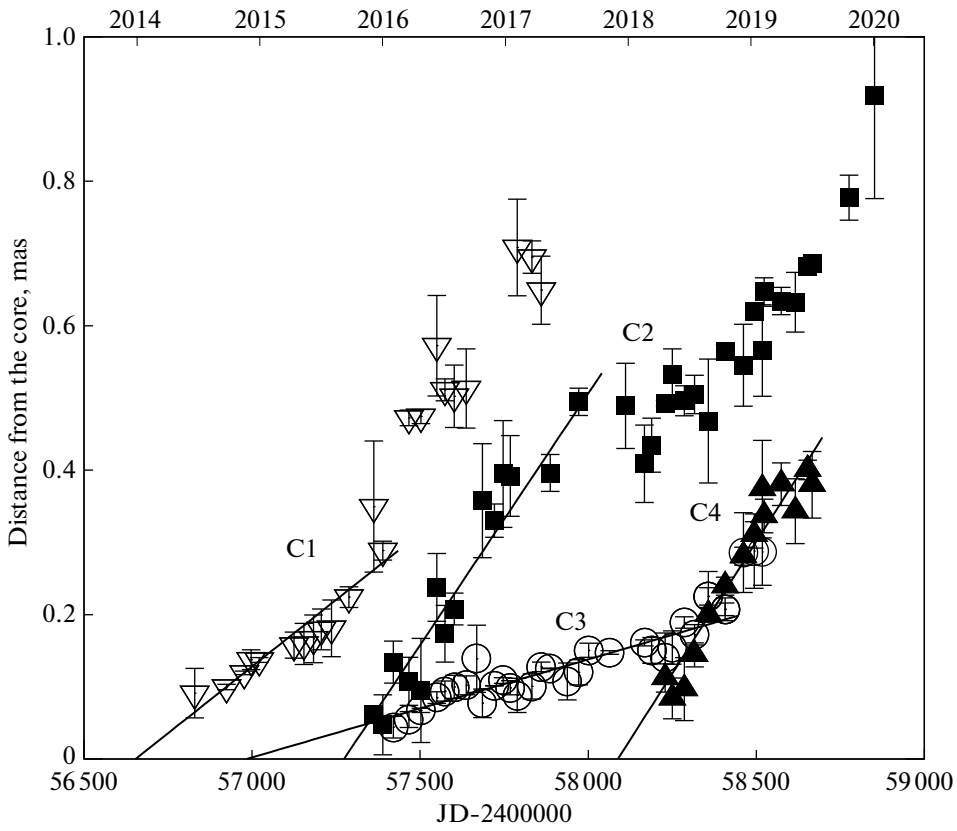

Fig. 9. Time-dependence of location of superluminal components on millisecond scale.

as well as activity in the optical and/or gamma ranges. Component C1 passed through the jet nucleus during the flare in the optical range, while there was no significant activity in the gamma range. Component C2 passed through the nucleus when an increase of activity in the gamma range was observed, but it is impossible to judge the optical contribution during this time interval, since data are not available. Component C3 appeared before the flare in the optical range in early 2015, which was accompanied by a bright flare in the radio jet nucleus and an increase of flux density in the gamma range. The fastest component C4 (with the velocity of ~13 s) appeared during the period of strong activity of the object, which occurred at the end of 2017 and lasted for almost entire 2018. The passage of the C4-component through the jet core coincided with the most powerful flare in the gamma and optical ranges with a maximum at JD ~ 2458100. This powerful flash was followed by a second, slightly less bright flash, which was also recorded in the optical and gamma ranges (with maximum on JD ~ 2458250). At the same time, it can be seen on the light curve that, when the C4-component began to be resolved separately from the nucleus, in the C3-component, which appeared earlier and moved at a much lower velocity (~3 s), a flare occurred during the period JD2458200–2458300, which coincided with the activity in two other ranges. The average positional angle of the components C3 and C4, moving to the northwest (~–50° and –40°), differs significantly from the angles of the previous components (~30° and ~4° for C1 and C2), which moved mainly to the northeast. This explains the influence of geometric effects during the active behavior of the object in 2017–2018. Thus, it can be

Table 4. Apparent velocities and other characteristics of detected components

Component	μ, ms/yr	β_{app}, s	T_0, JD 2400000+	$\langle F \rangle$, Ju	$\langle \theta \rangle$, deg
C1	0.136 ± 0.014	5.56 ± 0.58	56656 ± 16	0.08 ± 0.07	26 ± 21
C2	0.279 ± 0.003	11.38 ± 0.14	57274 ± 15	0.13 ± 0.20	4 ± 5
C3	0.081 ± 0.002	3.30 ± 0.08	56974 ± 15	0.59 ± 0.32	–52 ± 21
C4	0.314 ± 0.006	12.80 ± 0.26	58091 ± 12	0.11 ± 0.09	–40 ± 15

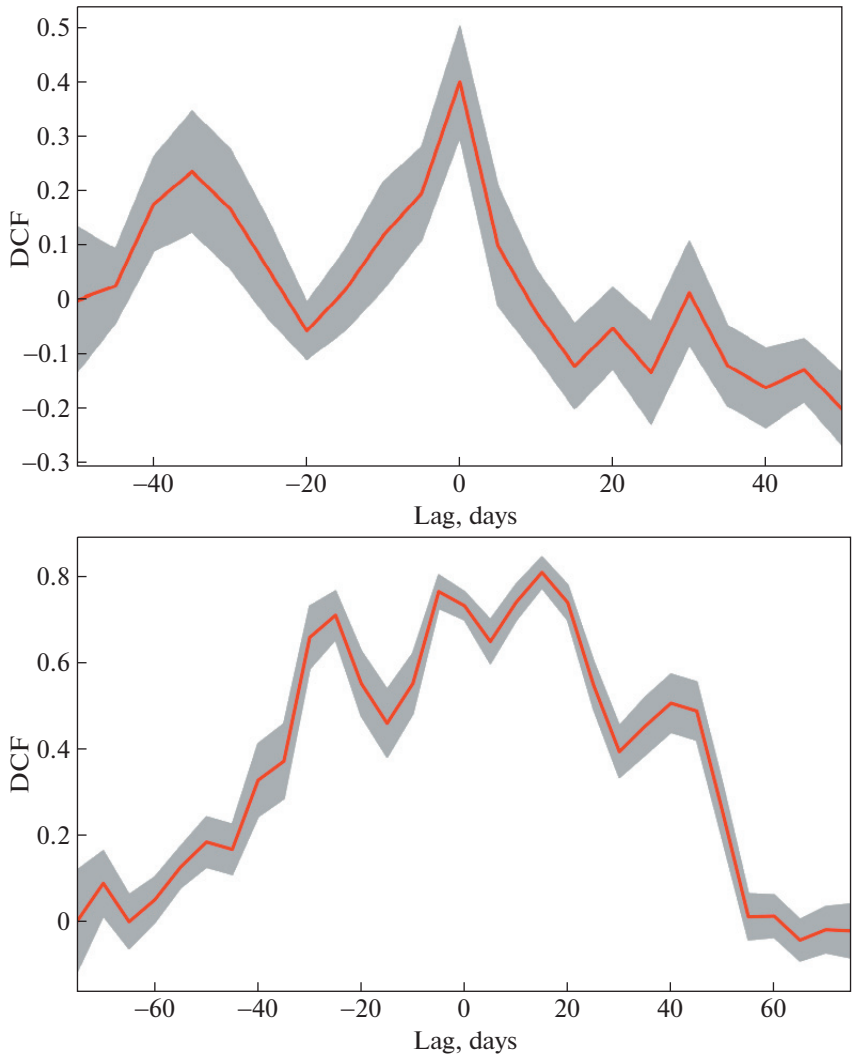

Fig. 10. Computation results of DCF for intervals of time from the beginning of observations to JD 2456900 (upper panel) and after this date (lower panel).

assumed that the main flare with a maximum at JD ~ 2458100 occurred in the jet nucleus when the C4-component passed through it, and the subsequent flare with a maximum at JD ~ 2458250 was associated with the interaction of components C3 and C4.

Examination of the bottom panel in Fig. 3 shows that strong flares in visual and gamma ranges far from always coincide in time. Results of calculating the discrete correlation function (DCF [16]) for the interval up to JD2457650 (top panel) and for the period of high activity 2017–2018 (bottom panel) are shown in Fig. 10. In the first case, the correlation is small, but the time delay is definitely absent, which indicates the same localization of the sources of optical and gamma radiation in the blazar jet. The bottom panel indicates a strong correlation between changes in the visual and gamma ranges. The line shows a complex structure, also symmetric about zero time delay.

The power-law nature of SED and the observed high degree of polarization leave no doubt about the synchrotron nature of the variable sources responsible for the activity. Data in Table 2 indicate the differences in the SED of the variable component at different time intervals. The differences in the spectral indices, although insignificantly, exceed the errors of their determination. This, as well as the difference of the average value of the spectral index from that found in [4], does not allow to explain the variability of the flux by geometrical factors *only* (variation of the Doppler effect due to variation of the line of sight and the direction of the subluminal motion of the emitting ensemble of electrons). The distributions of electrons over energy in the ensembles at different time intervals should be different.

Consideration of Table 3 shows that the values of the degree of polarization for the sources identified in

the model of a single variable component are not very large, while they differ strongly between different directions. But it is important to note that the data in Table 3 reflect the average trend in the change in the polarization parameters for a given time interval only. In fact, the degrees of polarization of individual components can be larger, since several sources of polarized radiation with different directions of polarization, caused by the inhomogeneity of the magnetic field, can operate simultaneously. Apparently, this explains previously noted small values of the degree of polarization at high fluxes (Fig. 7) in the most powerful flare.

A detailed study of the polarization behavior of an object is possible only after obtaining continuous high-precision observations. This is especially important for the studies of ultra-fast variations. The results of the first attempts of such observations for one of the blazars (S5 0716+714) were published recently [17].

ACKNOWLEDGMENTS

The authors acknowledge the staff workers of St. Petersburg State University who participated in observations and the group from Boston University for providing the results of optical monitoring. The final versions of results of photometric and polarization monitoring were compiled by V.M. Larionov. The study made use of the data of the monitoring in Boston University VLBA-BU-BLAZAR (http://www.bu.edu/blazars/), which is financed by NASA grant as a part of the program "Fermi Guest Investigator Program." The authors acknowledge S.G. Jorstad and Z. Weaver for useful discussion.

FUNDING

The study was supported by RFBR grant (contract no. 17-12-01029).

REFERENCES

1. M.-P. Veron-Cetty and P. Veron, Astron. Astrophys. **518**, A10 (2010).
2. M. L. Sitko, G. D. Schmidt, and W. A. Stein, Astrophys. J. Suppl. **59**, 323 (1985).
3. P. S. Smith, T. J. Balonek, R. Elston, and P. A. Heckert, Astrophys. J. Suppl. **64**, 459 (1987).
4. V. A. Gagen-Torn, S. G. Marchenko, and O. V. Mikolaichuk, Astrofizika **32**, 429 (1990).
5. S. G. Jorstad, A. P. Marscher, D. A. Morozova, et al., Astrophys. J. **846**, 98 (2017).
6. A. A. Abdo, M. Ackermann, M. Ajello, W. B. Atwood, et al., Astrophys. J. **700**, 597 (2009).
7. V. A. Hagen-Thorn, V. M. Larionov, N. V. Efimova, E. I. Hagen-Thorn, A. A. Arkharov, A. di Paola, M. Dolci, L. O. Takalo, A. Sillanpää, and L. Ostorero, Astron. Rep. **50**, 458 (2006).
8. S. G. Jorstad, A. P. Marscher, P. Smith, et al., Astrophys. J. **773**, 147 (2013).
9. A. R. J. Mead, K. R. Ballard, P. W. J. L. Brand, J. H. Hough, C. Brindle, and J. A. Bailey, Astron. Astrophys. Suppl. **83**, 183 (1990).
10. W. B. Atwood, A. A. Abdo, M. Ackermann, et al., Astrophys. J. **697**, 1071 (2009).
11. S. G. Jorstad, A. P. Marscher, M. L. Lister, A. M. Stirling, et al., Astron. J. **130**, 1418 (2005).
12. J.-Y. Wang, T. An, W.A. Baan, and X.-L. Lu, Mon. Not. R. Astron. Soc. **443**, 58 (2014).
13. V. A. Hagen-Thorn and S. G. Marchenko, Baltic Astron. **8**, 575 (1999).
14. V. A. Hagen-Thorn, V. M. Larionov, S. G. Jorstad, A. A. Arkharov, E. I. Hagen-Thorn, N. V. Efimova, L. V. Larionova, and A. P. Marscher, Astrophys. J. **672**, 40 (2008).
15. V. M. Larionov, S. G. Jorstad, A. P. Marscher, M. Villata, C. M. Raiteri, et al., Mon. Not. R. Astron. Soc. **492**, 3829 (2020).
16. R. A. Edelson and J. H. Krolik, Astrophys. J. **333**, 646 (1988).
17. E. S. Shablovinskaya and V. L. Afanasiev, Mon. Not. R. Astron. Soc. **482**, 4322 (2019).

Translated by L. Yungelson